Pulse shape of ultrashort intense laser reflected from a plasma mirror

Xulei Ge (葛绪雷)[1,2,3], Xiaohui Yuan (远晓辉)[2,3,*], Yuan Fang (方 远)[2,3], Wenqing Wei (魏文青)[2,3], Su Yang (杨 骕)[2,3], Feng Liu (刘 峰)[2,3,], Min Chen (陈 民)[2,3], Li Zhao (赵 利)[1], Zhengming Sheng (盛政明)[2,3,4], and Jie Zhang (张 杰)[2,3]**

[1]*State Key Laboratory of Surface Physics and Department of Physics, Fudan University, Shanghai 200433, China*
[2]*Key Laboratory for Laser Plasmas (MoE) and School of Physics and Astronomy, Shanghai Jiao Tong University, Shanghai 200240, China*
[3]*Collaborative Innovation Center of IFSA (CICIFSA), Shanghai Jiao Tong University, Shanghai 200240, China*
[4]*SUPA, Department of Physics, University of Strathclyde, Glasgow G4 0NG, United Kingdom*
**Corresponding author: xiaohui.yuan@sjtu.edu.cn; **corresponding author: liuf001@sjtu.edu.cn*
Received April 21, 2018; accepted August 27, 2018; posted online September 20, 2018

The temporal profiles of high-power short-pulse lasers reflected from self-induced plasma mirrors (PMs) were measured with high temporal resolution in the sub-picosecond window. The leading front shape of the laser pulse is found to depend sensitively on the laser fluence on the PM surface. Spectral modulation plays a key role in pulse profile shaping. Our findings will extend our knowledge on properly using PMs.
OCIS codes: 320.5540, 320.7080, 350.5400.
doi: 10.3788/COL201816.103202.

With the increase of achievable intensity of high-power lasers, the requirement of higher temporal contrast, defined as the intensity ratio of the leading front to the main peak, has been a growing issue in laser–plasma interaction experiments[1,2]. Nanosecond-duration amplified spontaneous emission (ASE) and shorter-duration prepulses are sources of the background noise. The latter could be attributed to the nature of non-Gaussian-distributed optical spectrum and the residual spectral chirp or non-ideal optics in the laser chain. As a robust technique, the plasma mirror (PM) has been routinely used to improve the laser temporal contrast. The initially transparent PM substrate is employed to transmit the ASE and prepulses and to reflect the main pulse when the substrate is ionized to the plasma state. A number of experiments and theoretical work have been performed to understand dynamics of the PM and to assess its performances[3–5]. Laser contrasts in the nanosecond and picosecond regimes were normally characterized by comparing the laser temporal profiles between whether the PM is adopted or not. Two orders of magnitude enhancement in the contrast were reported for both temporal regimes. Further improvements were achieved with the cascaded double-PM scheme[6,7].

PM-enhanced higher contrast lasers are superior in laser-driven ion acceleration and have the possibility to explore novel acceleration mechanisms with an ultrathin target, i.e., radiation pressure acceleration (RPA)[8,9], breakout afterburner (BOA)[10]. Recent researches show that multiple mechanisms may dominate over time due to intra-pulse intensity temporal evolution[11,12]. The prepulse-free lasers, with an additional laser pulse serving as a controllable prepulse, offer the opportunity for controlling and optimizing higher-order harmonic generation (HHG)[2,13]. The sensitive dependence of ion acceleration and HHG on the exact laser pulse shape poses severe requirements on well characterization and control of the complete laser temporal profiles. Two theoretical works suggested that the PM could steepen the femtosecond rising front for an ideal (Gaussian-distributed) input laser pulse[6,14]. However, the temporal profile of the laser pulse reflected from the PM in the sub-picosecond regime and its sensitivity to experimental conditions were scarcely investigated experimentally so far[6]. The optimized PM performance was operationally chosen based on measurements of the integrated reflectivity and evaluations of the far-field beam qualities by varying the laser fluences on the PM surface[5]. The pulse duration after employing the PM was thought to be unchanged in analyzing experimental results.

In this Letter, we show that the temporal shape of the laser pulse is sensitively influenced by laser fluence on the PM surface. A cleaner pulse can be produced using smaller laser fluence at the expense of reflectivity. The role of plasma formation close to the main pulse on the pulse shape is discussed. The results will extend our knowledge on proper utility of the PM technique for temporal contrast improvement and applications.

This experiment was carried out using the high-power Ti:sapphire laser at Shanghai Jiao Tong University. The lasers could deliver pulses with energy up to 5 J in 10 Hz and pulse duration of ~25 fs (full width at half-maximum, FWHM). The schematic of the PM setup and main diagnostics are shown in Fig. 1(a). Using an $f/10$ off-axis parabola mirror (OAP1), the incident p-polarized beam is focused on the PM to a spot millimeters in diameter at an incident angle of 10°. To minimize the reflection of the ASE and prepulses, anti-reflection (AR) coated BK7 glass is used as a PM, which has an initial reflectivity

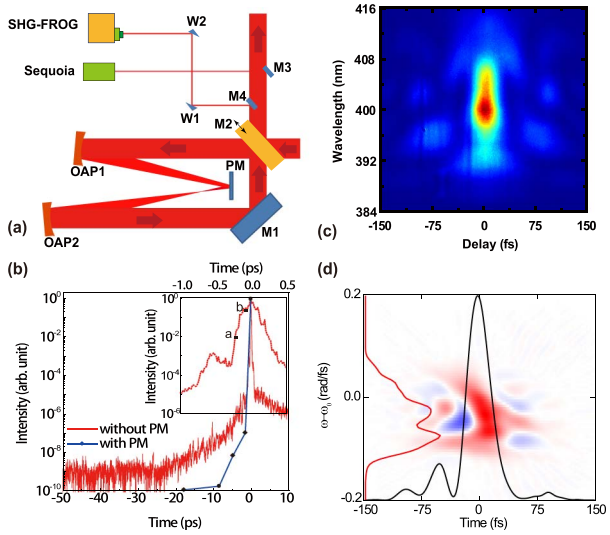

Fig. 1. (a) Schematic of the experimental setup. Two identical off-axis parabola mirrors, OAP1 and OAP2, are used to focus and recollimate the laser beam. The laser pulse temporal profiles are measured with SHG-FROG and Sequoia. W1, W2 are wedged fused silica plates, and M1–M4 are HR mirrors. M2 is mounted on a motorized linear stage. PM stands for plasma mirror. (b) The laser contrast measurement in a 60 ps window using Sequoia. The inset is the zoom-in profile from −1 to 0.5 ps. The 'a' and 'b' correspond to the estimated PM trigger times for laser fluences $F_{\rm pm}$ of 140.0 J/cm^2 and 6.5 J/cm^2, respectively. Example results of (c) retrieved FROG trace and (d) the corresponding Wigner distribution of laser pulse without a PM.

of less than 0.2% in the range of 740–860 nm. The damage threshold of the coating is about 4 J/cm^2[6]. After the PM, the specularly reflected divergent beam is recollimated by an identical OAP mirror (OAP2). A high-reflection (HR) dielectric mirror (M1) subsequently reflects the recollimated beam to the target chamber for characterizations or experiments of proton acceleration and HHG. In this work, the laser fluence on the PM, $F_{\rm pm}$, is varied from 5 J/cm^2 to 150 J/cm^2 by changing the on-surface beam diameter at a fixed laser energy of 1.8 J. A motorized HR dielectric mirror M2 is used to bypass the PM system[15].

The reflected beam from the PM system is sampled by two 20-mm-diameter pick-up mirrors (M3 and M4) for pulse temporal profile measurements. In the subpicosecond regime, it is single-shot measured using a frequency-resolved optical gating (FROG, GRENOUILLE, Swamp Optics, LLC.) device. The device is based on second harmonic generation (SHG), having 1.2 fs temporal and 1.3 nm spectral resolutions, respectively. The temporal window is 300 fs. Wedged plates and a 1-mm-thick vacuum window both made of fused silica are used to reduce the laser energy into individual diagnostics and minimize the transmission-induced dispersion and B integral[16]. Due to the time direction ambiguity of the autocorrelation process, two possible pulses for each FROG trace could be retrieved. By positively chirping the pulse via inserting a thick glass plate into the beam path, the leading and falling sides could be distinguished[17]. The temporal profile, i.e., intensity contrast, in the sub-nanosecond domain is measured with a scanning high-dynamic-range third-order cross-correlator (Sequoia, Amplitude Technologies)[18].

The Sequoia measurement results are shown in Fig. 1(b). The initial temporal intensity contrast is better than 10^{-8} before −20 ps and better than 10^{-5} before −1 ps. The contrast could be improved up to 10^{-10} at −10 ps and 10^{-7} at −1 ps with the PM. This temporal contrast improvement allows efficient proton acceleration and HHG[13,18]. A close zoom-in profile near the main peak is shown in the inset of Fig. 1(b) for the case without a PM. It provides information of the PM triggering time, for example, 'a' and 'b' corresponding to $F_{\rm pm} = 140.0$ J/cm^2 and $F_{\rm pm} = 6.5$ J/cm^2, respectively.

Figure 1(c) is the raw FROG image of the input laser pulse, i.e., without the PM. The FROG trace contains both amplitude and phase information of the laser pulse, thus allowing the pulse profile to be uniquely retrieved. To visually present the intensity profile of the pulse and the instantaneous frequency, the Wigner distribution, which represents photon distribution in time-frequency space for the retrieved pulse shape, is calculated as[17]

$$W(t,\omega) = \int_{-\infty}^{\infty} E(t+t'/2)E^*(t-t'/2)\exp(-i\omega t')\,{\rm d}t',$$

where $E(t)$ is the time-varying electric field, ω is the laser frequency, and t' is the time lag. The Wigner distribution of a laser pulse without a PM is shown in Fig. 1(d). High-order dispersions are observed. The profiles of the temporal intensity $I(t) = \int W(t,\omega)\,{\rm d}\omega$ and spectrum of the pulse $S(\omega) = \int W(t,\omega)\,{\rm d}t$ are also plotted. The spectrum is obviously not Gaussian distributed. Two little bulges ('prepulses') appear prior to the main peak with relative intensity levels of ∼5% and ∼18% to the main peak, respectively. The two prepulses are formed due to the combined effects of high-order residual dispersions and non-Gaussian-distributed laser spectrum.

The multiple pulses may have an impact on the laser–plasma interaction in two folds. The preceding intense pulses may produce a pinching magnetic field to collimate the successive laser-produced fast electrons[19,20]. Spectral enhancement of the laser-accelerated proton beam may be achieved with double pulses[21,22]. On the other hand, prepulse-free lasers are of prime importance for many topics of laser–solid interactions[9,10,23]. The temporal-shaped laser pulse with a sharp front is required to satisfy a near-solid-density short-scalelength plasma[24,25].

The measured laser temporal profiles with respect to $F_{\rm pm}$ are compared in Fig. 2. Figure 2(a) is analogous to the initial input pulse, i.e., the temporal profile shown in Fig. 1(d). With decreasing $F_{\rm pm}$, obvious pulse shaping occurs in the leading front. The level of the prepulses gradually decreases. The prepulses reduce to a single peak for $F_{\rm pm} < 23.8$ J/cm^2 [Fig. 2(c)] and vanish eventually for $F_{\rm pm} < 6.5$ J/cm^2 [Fig. 2(f)]. The shape and amplitude of the falling edge of the main pulse and postpulse are nearly

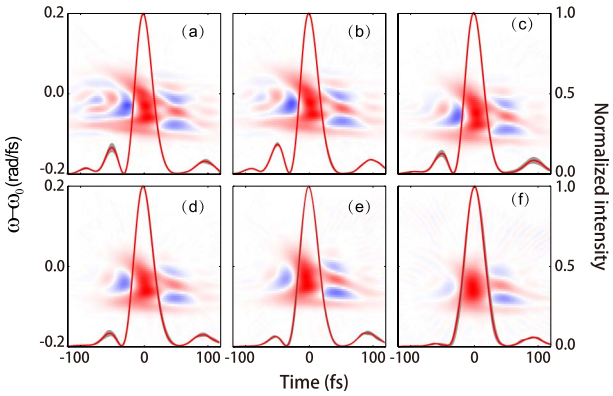

Fig. 2. Wigner distribution (left axis) and temporal profiles (right axis) of the laser pulse after reflection from the PM with F_{pm} equal to (a) 140.0 J/cm^2, (b) 50.0 J/cm^2, (c) 23.8 J/cm^2, (d) 14.0 J/cm^2, (e) 9.2 J/cm^2, and (f) 6.5 J/cm^2. The intensity is normalized to the peak value at $t = 0$ fs. The shaded area in each plot is due to the shot-to-shot fluctuations.

unchanged. The prepulse suppression as a function of F_{pm} is easy to understand. When the fluence is high, it is too early to trigger the PM so that the two prepulses are fully reflected by the preformed plasma surface. The earlier formed plasma has equal effects on reflecting the main pulse and prepulses. The later trigger of the reflective PM surface at low fluence allows more leading parts of the laser to transmit. The rough trigger times for the cases of Figs. 2(a) and 2(f) are labelled in the inset of Fig. 1(b).

Though the main peak pulses are similar in Fig. 2, they have measurable changes on the rising edge. It shows slower up-ramp in contradiction to the steepened profile reported before[14]. We should mention that this difference is due to the different initial laser profiles, i.e., ideal Gaussian profile in simulation and complex pulse shape in reality. The duration of the reflected pulse from the PM is quantified with two methods. The FWHM, the most frequently used definition, of the pulse duration is presented in Fig. 3. The initial laser has a T_{FWHM} of 31 fs, which is larger than the best condition (Fourier-transform-limited pulse) due to the uncompensated high-order dispersion. The T_{FWHM} increases with decreasing F_{pm}. It is essentially

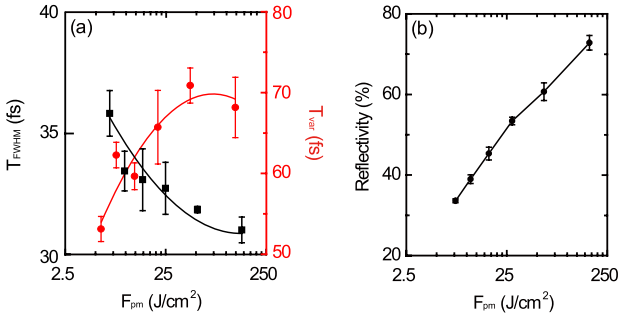

Fig. 3. (a) Pulse durations measured with FWHM (T_{FWHM}) and the second-order moment (T_{var}) methods. The solid lines are drawn to guide eyes. (b) Integrated reflectivity of the PM-reflected laser pulse as a function of F_{pm}.

the width of the main laser peak pulse in our cases and insensitive to the weak pedestals and prepulses. For the complicated pulse profile, a definition based on the second-order moment, i.e., variance, of the temporal profile is more appropriate[26]. The second moment of the beam temporal profile $I(t)$ could be calculated in the form $\tau^2 = \int_{-\infty}^{\infty}(t-t_0)^2 I(t)\,\mathrm{d}t / \int_{-\infty}^{\infty} I(t)\,\mathrm{d}t$, where $t_0 = \int_{-\infty}^{\infty} t \cdot I(t)\,\mathrm{d}t / \int_{-\infty}^{\infty} I(t)\,\mathrm{d}t$. The calculated duration with variance, $T_{\mathrm{var}} = 2\tau$, is also plotted in Fig. 3(a). It shows an opposite trend to T_{FWHM}. This agrees with the fact that the intensity of the pedestals in the leading part of the laser pulse increases with laser fluence on the PM and plays an increasingly important role in T_{var}. Note that the integrated reflectivity decreases by a factor of 2 from 70% to 32% when F_{pm} decreases from 140.0 J/cm^2 to 6.5 J/cm^2. To check whether the pulse-duration variation is due to the laser energy loss when reflecting from the PM, the laser pulse was directly measured by the reflecting laser with M2 for different laser energy (i.e., without using the PM). We found that the pulse duration is nearly constant for two-fold variations of laser energy. This indicates that the pulse-duration change is not an instrumental issue.

To understand the pulse shape change, the spectral intensity and phase of PM-reflected laser pulses from the retrieved FROG trace are compared in Figs. 4(a)–4(f), which correspond to the same conditions in Figs. 2(a)–2(f). Spectral narrowing is observed with decreasing F_{pm}. Spectral intensity was suppressed at some specific wavelength, e.g., at 775 nm, while the spectral phase has no significant change. The modulations on the laser spectrum could give rise to the pulse shape change and can be explained as follows: the leading front of the laser pulse will ionize the PM surface and get dissipated when its intensity is higher than the ionization threshold of the PM surface. The lower laser fluence results in a later triggering of the PM, and therefore, the more dissipated leading front. Since the rise time of the PM's reflectivity (the time from triggering the PM to reaching

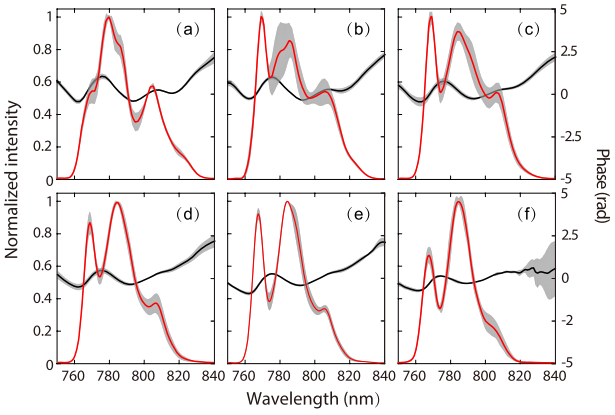

Fig. 4. Retrieved spectral intensity (red line) and phase (black line) of the PM-reflected laser beam with the same laser fluence as in Fig. 2. The shaded area in each plot is due to shot-to-shot fluctuations.

the maximum reflectivity) is about a few hundreds of femtoseconds determined by the time required for ionizing the PM surface to critical density[27,28], significant effects of PM formation on non-ideally compressed pulse reflection are expected. The nonlinear spatio-temporal coupling may also cause the pulse shape change as a result of the beam sampling[6]. This effect is more pronounced for the case when near-field distribution is distorted. The distribution is likely to be deteriorated for high laser fluence. Therefore the spatio-temporal distortion has a negligible effect on pulse-duration change.

To further understand the spectral modulations presented in Fig. 4, we defined the modulation depth as the ratio of spectral intensity difference after reflection from the PM to the spectral intensity of the incident laser, formulated as $\Gamma = (I_{re} - I_{in})/I_{in}$. Here, I_{re} and I_{in} are the spectral intensity of the PM-reflected pulse and the incident pulse, respectively. Figure 5 shows the examples of Γ with $F_{pm} = 50.0$ J/cm^2 [Fig. 5(a)] and $F_{pm} = 9.2$ J/cm^2 [Fig. 5(b)]. The leading spectral components in time have larger Γ when forming plasma. The group delay $t = \mathrm{d}\phi/\mathrm{d}\omega$, where ϕ is the spectral phase, and ω is the laser frequency, is also compared. The group delay shows complex high-order dispersions, which are usually difficult to be compensated by only tuning the grating compressor. There is no significant change in group delay of the laser pulse with or without PM, as shown by red and a dash line in Fig. 5. The tendency of t is consistent with Γ. The leading components of the spectra interact earlier with the PM substrate and have smaller reflection, which will cause spectrum erosion. This causes the spectral modulations shown in Fig. 4, and the eroded spectrum therefore results

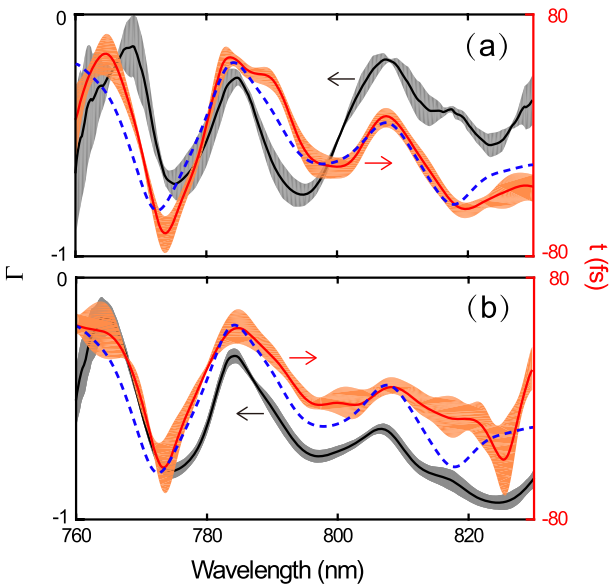

Fig. 5. Modulation depth Γ (black line) and group delay t (red line) for two laser fluence examples of (a) $F_{pm} = 50.0$ J/cm^2 and (b) $F_{pm} = 9.2$ J/cm^2. The dashed lines are the reference group delays for the laser pulse without a PM. The shaded areas are the standard deviations due to shot-to-shot fluctuations.

in the increase of the pulse duration, as shown in Fig. 3(a). The consistency of Γ with the group delay t implies that the measurement of Γ could be used to infer the laser spectral phase.

In summary, we have measured the temporal profiles of laser pulses after reflection from a self-induced PM in the sub-picosecond temporal window. We find that the prepulses within a few hundred femtoseconds before the main peak could be suppressed by varying the fluence on the PM. The suppression is determined by the group delay of the main pulse. Experimental results suggest that special cares should be taken when non-ideally compressed pulses are used in experiments. Our findings will extend our knowledge on the proper utility of the PM technique for temporal contrast improvement and in applications of laser-driven particle acceleration and radiation source development.

This work was supported by the National Basic Research Program of China (No. 2013CBA01502), the National Natural Science Foundation of China (Nos. 11721091, 11205100, and 11305103), and the National Key Scientific Instrument Development Project (No. 2012YQ030142).

References

1. D. Neely, P. Foster, A. Robinson, F. Lindau, O. Lundh, A. Persson, C.-G. Wahlström, and P. McKenna, Appl. Phys. Lett. **89**, 021502 (2006).
2. S. Kahaly, S. Monchocé, H. Vincenti, T. Dzelzainis, B. Dromey, M. Zepf, P. Martin, and F. Quéré, Phys. Rev. Lett. **110**, 175001 (2013).
3. H. C. Kapteyn, M. M. Murnane, A. Szoke, and R. W. Falcone, Opt. Lett. **16**, 490 (1991).
4. G. Doumy, F. Quéré, O. Gobert, M. Perdrix, P. Martin, P. Audebert, J. C. Gauthier, J.-P. Geindre, and T. Wittmann, Phys. Rev. E **69**, 1539 (2004).
5. B. Dromey, S. Kar, M. Zepf, and P. Foster, Rev. Sci. Instrum. **75**, 645 (2004).
6. T. Wittmann, J. P. Geindre, P. Audebert, R. S. Marjoribanks, J. P. Rousseau, F. Burgy, D. Douillet, T. Lefrou, K. T. Phuoc, and J. P. Chambaret, Rev. Sci. Instrum. **77**, 083109 (2006).
7. A. Lévy, T. Ceccotti, P. D'Oliveira, F. Réau, M. Perdrix, F. Quéré, P. Monot, M. Bougeard, H. Lagadec, P. Martin, J.-P. Geindre, and P. Audebert, Opt. Lett. **32**, 310 (2007).
8. X. Q. Yan, C. Lin, Z. M. Sheng, Z. Y. Guo, B. C. Liu, Y. R. Lu, J. X. Fang, and J. E. Chen, Phys. Rev. Lett. **100**, 135003 (2008).
9. A. Henig, S. Steinke, M. Schnürer, T. Sokollik, R. Hörlein, D. Kiefer, D. Jung, J. Schreiber, B. M. Hegelich, X. Q. Yan, J. Meyer-Ter-Vehn, T. Tajima, P. V. Nickles, W. Sandner, and D. Habs, Phys. Rev. Lett. **103**, 245003 (2009).
10. L. Yin, B. J. Albright, K. J. Bowers, D. Jung, J. C. Fernández, and B. M. Hegelich, Phys. Rev. Lett. **107**, 045003 (2011).
11. H. Padda, M. King, R. J. Gray, H. W. Powell, B. Gonzalez-Izquierdo, L. C. Stockhausen, R. Wilson, D. C. Carroll, R. J. Dance, D. A. MacLellan, X. H. Yuan, N. M. H. Butler, R. Capdessus, M. Borghesi, D. Neely, and P. McKenna, Phys. Plasmas. **23**, 063116 (2016).
12. A. Higginson, R. J. Gray, M. King, R. J. Dance, S. D. R. Williamson, N. M. H. Butler, R. Wilson, R. Capdessus, C. Armstrong, J. S. Green, S. J. Hawkes, P. Martin, W. Q. Wei, S. R. Mirfayzi, X. H. Yuan,

S. Kar, M. Borghesi, R. J. Clarke, D. Neely, and P. McKenna, Nat. Commun. **9**, 724 (2018).
13. J. Gao, F. Liu, X. Ge, Y. Deng, G. Zhang, Y. Fang, W. Wei, S. Yang, X. Yuan, M. Chen, Z. Sheng, and J. Zhang, Chin. Opt. Lett. **15**, 081902 (2017).
14. S. S. Bulanov, A. Macchi, A. Maksimchuk, T. Matsuoka, J. Nees, and F. Pegoraro, Phys. Plasmas **14**, 093105 (2007).
15. Y. Fang, X. Ge, S. Yang, W. Wei, T. Yu, F. Liu, M. Chen, J. Liu, X. Yuan, Z. Sheng, and J. Zhang, Plasma Phys. Control. Fusion **58**, 075010 (2016).
16. S. Palaniyappan, R. C. Shah, R. Johnson, T. Shimada, D. C. Gautier, S. Letzring, D. Jung, R. Hörlein, D. T. Offermann, J. C. Fernandez, and B. M. Hegelich, Rev. Sci. Instrum. **81**, 10E103 (2010).
17. J. Schreiber, C. Bellei, S. P. D. Mangles, C. Kamperidis, S. Kneip, S. R. Nagel, C. A. J. Palmer, P. P. Rajeev, M. J. V. Streeter, and Z. Najmudin, Phys. Rev. Lett. **105**, 235003 (2010).
18. X. Ge, Y. Fang, S. Yang, W. Wei, F. Liu, P. Yuan, J. Ma, L. Zhao, X. Yuan, and J. Zhang, Chin. Opt. Lett. **16**, 013201 (2018).
19. A. P. L. Robinson, M. Sherlock, and P. A. Norreys, Phys. Rev. Lett. **100**, 025002 (2008).
20. R. H. H. Scott, C. Beaucourt, H.-P. Schlenvoigt, K. Markey, K. L. Lancaster, C. P. Ridgers, C. M. Brenner, J. Pasley, R. J. Gray, I. O. Musgrave, A. P. L. Robinson, K. Li, M. M. Notley, J. R. Davies, S. D. Baton, J. J. Santos, J.-L. Feugeas, P. Nicolaï, G. Malka, V. T. Tikhonchuk, P. McKenna, D. Neely, S. J. Rose, and P. A. Norreys, Phys. Rev. Lett. **109**, 015001 (2012).
21. K. Markey, P. McKenna, C. M. Brenner, D. C. Carroll, M. M. Günther, K. Harres, S. Kar, K. Lancaster, F. Nürnberg, M. N. Quinn, A. P. L. Robinson, M. Roth, M. Zepf, and D. Neely, Phys. Rev. Lett. **105**, 195008 (2010).
22. G. G. Scott, V. Bagnoud, C. Brabetz, R. J. Clarke, J. S. Green, R. I. Heathcote, H. W. Powell, B. Zielbauer, T. D. Arber, P. McKenna, and D. Neely, New J. Phys. **17**, 033027 (2015).
23. B. Dromey, S. Rykovanov, M. Yeung, R. Hörlein, D. Jung, D. C. Gautier, T. Dzelzainis, D. Kiefer, S. Palaniyppan, R. Shah, J. Schreiber, H. Ruhl, J. C. Fernandez, C. L. S. Lewis, M. Zepf, and B. M. Hegelich, Nat. Phys. **8**, 804 (2012).
24. F. Pegoraro and S. V. Bulanov, Phys. Rev. Lett. **99**, 065002 (2007).
25. S. S. Bulanov, C. B. Schroeder, E. Esarey, and W. P. Leemans, Phys. Plasmas. **19**, 093112 (2012).
26. J. C. Diels and W. Rudolph, *Ultrashort Laser Pulse Phenomena* (Elsevier, 2006).
27. F. Quéré, C. Thaury, J.-P. Geindre, G. Bonnaud, P. Monot, and P. Martin, Phys. Rev. Lett. **100**, 095004 (2008).
28. Y. Cai, W. Wang, C. Xia, J. Liu, L. Liu, C. Wang, Y. Xu, Y. Leng, R. Li, and Z. Xu, Phys. Plasmas **16**, 103104 (2009).